Available online at http://scik.org
J. Math. Comput. Sci. 11 (2021), No. 2, 1256-1285
https://doi.org/10.28919/jmcs/5123
ISSN: 1927-5307

AN AUTOMATED OPTIMAL VACCINATION CONTROL WITH A MULTI-REGION SIR EPIDEMIC MODEL

ABDELHADI ABTA[1], HAMZA BOUTAYEB[2], SARA BIDAH[2,*], OMAR ZAKARY[2], MUSTAPHA LHOUS[3], MOSTAFA RACHIK[2]

[1]Department of Mathematics and Computer Science, Poly-disciplinary Faculty, Cadi Ayyad University, P.O. Box 4162, Safi, Morocco

[2]Laboratory of Analysis Modelling and Simulation, Department of Mathematics and Computer Science, Faculty of Sciences Ben M'Sik, Hassan II University of Casablanca, BP 7955, Sidi Othman, Casablanca, Morocco

[3]Laboratory of Modeling, Analysis, Control and Statistics, Department of Mathematics and Computer Science, Faculty of Sciences Ain Chock, Hassan II University of Casablanca, B.P 5366 Maarif Casablanca, Morocco

Abstract. Many mathematical models describing the evolution of infectious diseases underestimate the effect of the Spatio-temporal spread of epidemics. Currently, the COVID-19 epidemic shows the importance of taking into account the spatial dynamic of epidemics and pandemics. In this contribution, we consider a multi-region discrete-time epidemic model that describes the spatial spread of an epidemic within different geographical zones assumed to be connected with the movements of their populations. Based on the fact that there are several limitations in medical resources, the authorities and health decision-makers must define a threshold of infections in order to determine if a zone is epidemic or not yet. We propose a new approach of optimal control by defining new importance functions to identify affected zones and then the need for the control intervention there. Numerical results are provided to illustrate our findings by applying this new approach in two adjacent regions of Morocco,

*Corresponding author
E-mail address: sarabidah@gmail.com
Received October 18, 2020

the Casablanca-Settat and Rabat-Salé-Kénitra regions. We investigate different scenarios to show the most effective scenario, based on thresholds' values.

Keywords: vaccination; automated; SIR; epidemic; optimal control.

2010 AMS Subject Classification: 39A05, 39A45, 39A60, 93C35, 93C55.

1. INTRODUCTION

The field of epidemiology with the science of mathematics have been developed to study the transmission laws of epidemics [1]. Mathematical models provide the opportunity to understand how pandemics are spread and transmitted, taking into consideration the fact that these models present a mathematical translation of different hypotheses concerning the process of an epidemic transmission [2, 3]. However, in order to define outbreaks of various types of epidemics and to provide insights into disease control and policy formulations, mathematical formulations have been developed [4, 5]. Based on this data, effective control and preventive measures are suggested [6]. However, with the effect of spatio-temporal spread of epidemics, mathematical modeling should take into account the geographical criterion to show the spatial spread of an infectious disease within different geographical zones [7].

One of the basic models that was successfully investigated was the Kermack-Mckendrick model. To model an epidemic, the population being studied is divided into three classes labeled S, I, and R [8]:

(S) refers to susceptible people who are not infected, but the possibility of transmitting the infection is still existed.

(I) Infected individuals who receive the infection, and able to spread it by contact with other people.

(R) Recovered or removals are individuals who become immune after getting sick, or individuals who are isolated from other members of the group, or ones who die due to the disease [9, 10].

The transmission process of an epidemic is described when a population of susceptibles is being introduced into infectious individuals, then the infection is spread in the group through different modes of transmission [11, 12].

Various types of phenomena were analyzed and controlled by mathematical models, citing as example epidemics, Information dissemination, public opinion, and others.. [13, 14, 15, 16, 17, 18, 19, 20, 21, 22, 23, 24] .

Recently, the COVID-19 Virus has shown the necessity of taking into consideration the spatial dynamic of epidemics, and described how spatial heterogeneity affects the transmission dynamics of susceptible and infected populations [25, 7]. The Corona virus was reported firstly in Wuhan, China, the outbreak was greatly increased and moved to other Chinese cities and multiple countries, moving to other continents [26, 27, 28, 29]. In the history there were also many pandemics that show the spatio-temporal spread of pandemics such as the black plague [30], cholera [31], and others ... [32].

The discrete time multi-regional SIR model is a mathematical modeling of spatial and temporal spread of epidemics, an example of this model is made by [7], the multi-regional model is presented in multiple geographical areas to control the movements of the pandemic, and the infection can be spread from one region to another through travel. However, three main approaches are cited in [18], raise awareness by organizing vaccination campaigns, travel blocking movements coming from infected areas, and treatment. Other models are analyzed in this topic from many researchers in [33, 34].

In the history of all these diseases, we can notice their spread from one region to another, and recently the COVID-19 pandemic from its epicenter of Wuhan in China has spread to all parts of the world, which makes taking into account the spatial spread of diseases more important during modeling processes.

The authors in [7] present the first work in the modeling and control of spatio-temporal spread of an epidemic using a multi-region SIR discrete-time model, as a generalization of the concept of classical models and aiming at a description of the evolution of pandemics, Zakary et al proposed a new approach of modeling of the spread of epidemics from one area to another using finite-dimensional models for the Spatio-temporal propagation of epidemics as an alternative of the partial derivatives models which are of infinite dimension. The authors also suggested some control strategies such as awareness-raising, vaccination, and travel-restriction approaches that could prevent specific infectious diseases such as HIV / AIDS, Ebola, or other epidemics

in general [7, 35, 19, 18, 36], other researchers have shown the power and effectiveness of educational workshops and awareness programs in reducing the number of infected individuals [37, 38, 39].

In this paper, we propose a new optimal control approach mainly based on a multi-regions discrete-time system and a new form of multi-objective optimization criteria with importance indices and which is subject to multi-points boundary value optimal control problems. With more clarifications and essential details, we devise here a multi-regions discrete model for the study of the spread of an epidemic in M different regions, and analyze the effectiveness of vaccination (or awareness) optimal control strategies when vaccination (or awareness) campaigns are organized in infected zones. Here, we study the case when controls are applied to people who belong to all those regions and which are supposed to be reachable for every agent (nurse, doctor or media) who is responsible for the accomplishment of control strategies followed against the disease.

We consider an area as an infected zone if its number of infected individuals exceeds a threshold defined by the health decision-makers. Therefore, by varying the values of this threshold and then simulating the infection situation for different values of these thresholds shows that it is necessary to think about reducing the time between the first infection and the implementation of the control strategy. Unexpected results that in some situations the neighboring regions infected and its number of infections exceeds the threshold before the number of infections of the region source. This makes the implementation of the control strategies in the neighboring zones more important.

In our modeling approach we divided the studied area Ω into different zones that we call cells. A cell $C_j \in \Omega$ can represent a city, a country or a larger domain. These cells are supposed to be connected by movements of their populations within the domain Ω. We define also a neighboring cells C_k of the cell C_j all zones connected with C_j via every transport mean, thus a cell $C_j \in \Omega$ can have more than one neighboring cell. Here, we suppose that a cell can be infected due to movements of infected people which enter only from its neighboring zones.

We carry out the map of the studied area and then we use different threshold values in the controlled multi-region SIR model to simulate the epidemic spread within the Casablanca-Settat

FIGURE 1. The geographical studied zone Ω: (a) Discretization on two regions Casablanca-Settat and Rabat-Salé-Kénitra. (b) Discretization of the two regions on provinces with numbers. (c) Discretization of the whole studied zone on provinces with names. (d) Zoom in to Casablanca and its neighbors.

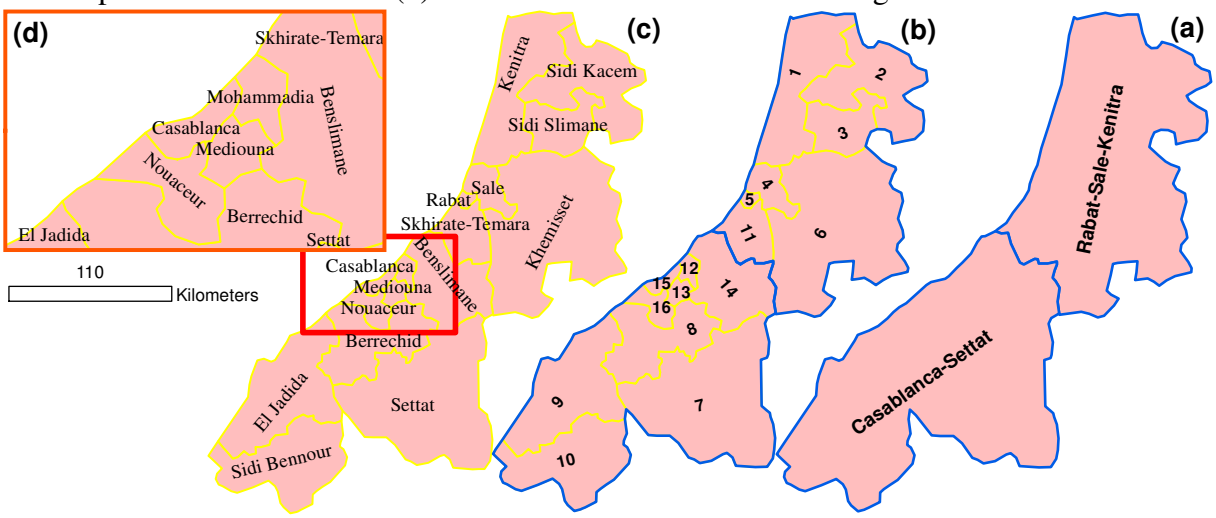

region and Rabat-Salé-Kénitra region illustrated in the Fig.1, by combining the ArcGIS and Matlab programs.

The paper is organized as follows: Section 2. presents the discrete-time multi-region SIR epidemic system. In Section 3., we announce theorems of the existence and characterization of the sought optimal controls functions related to the optimal control approach we propose. Finally, in section 4., we provide simulations of the numerical results applied to the Casablanca-Settat region and Rabat-Salé-Kénitra region as domain of interest.

2. MODEL DESCRIPTION AND DEFINITIONS

Based on same modeling assumptions of the reference [7], we assume that there are M geographical regions denoted C_j (sub-domains) of studied Ω

$$\Omega = \bigcup_{j=1}^{M} C_j$$

Nb	Zone	Population	Nb	Zone	Population	Nb	Zone	Population	Nb	Zone	Population
1	BEN SLIMANE	213398	5	CASABLANCA-ANFA	523279	9	BEN MSICK-SIDI OTHMANE	704365	13	KHENIFRA	220543
2	MOHAMMEDIA	170063	6	AL FIDA-DERB SULTAN	386700	10	SETTAT	847422	14	KHOURIBGA	480839
3	SIDI BERNOUSSI-ZENATA	268586	7	AIN CHOCK-HAY HASSANI	516261	11	EL JADIDA	970894	15	BENI MELLAL	869748
4	AIN SEBAA-HAY MOHAMMADI	520993	8	MACHOUAR CASABLANCA	3956	12	AIN CHOCK-HAY HASSANI	516261	16	AZILAL	454914

TABLE 1. Populations of the two regions: Casablanca-Settat and Rabat-Salé-Kénitra.

Where C_j can represent a city, a country or a larger domain. We note by $V(C_j)$, the vicinity set, composed by all neighboring cells of C_j given by

$$V(C_j) = \left\{ C_k \in \Omega \ / \ C_j \cap C_k \neq \emptyset \right\}$$

Where $C_j \cap C_k \neq \emptyset$ means that there exists at least one mean of transport between C_j and C_k. Note that this definition of $V(C_j)$ is more general where it defines a more general form of vicinity regardless the geographical location of zones.

For example, in the Table 1 we can see that the studied area consists of 16 zones.

The multi-regional discrete-time SIR model associated to C_j with $\varepsilon_i^{C_j} = 0$ (no control is introduced yet in C_j) is then

$$S_{i+1}^{C_j} = S_i^{C_j} - \sum_{C_k \in V(C_j)} \beta^{C_j^k} \frac{I_i^{C_k}}{N_i^{C_j}} S_i^{C_j} + \left(N_i^{C_j} - S_i^{C_j} \right) d_j \tag{1}$$

$$I_{i+1}^{C_j} = I_i^{C_j} + \sum_{C_k \in V(C_j)} \beta^{C_j^k} \frac{I_i^{C_k}}{N_i^{C_j}} S_i^{C_j} - \gamma_j I_i^{C_j} - d_j I_i^{C_j} - \alpha^{C_j} I_i^{C_j} \tag{2}$$

$$R_{i+1}^{C_j} = R_i^{C_j} + \gamma_j I_i^{C_j} - d_j R_i^{C_j} \tag{3}$$

where the disease transmission coefficient $\beta^{C_j^k} > 0$ is the proportion of adequate contacts in domain C_j between a susceptible from C_j $(j = 1, ..., M)$ and an infective from another domain C_k, d_j is the birth and death rate and γ_j is the recovery rate ans α^{C_j} is the proportion of mortality due to the disease. The biological background requires that all parameters be non-negative. $S_i^{C_j}$, $I_i^{C_j}$ and $R_i^{C_j}$ are the numbers of individuals in the susceptible, infective, and removed compartments of C_j at time i, respectively, and $N_i^{C_j} = S_i^{C_j} + I_i^{C_j} + R_i^{C_j}$ is the population size corresponding to domain C_j at time i. It is clear that the population size is not constant for all $i \geq 0$.

3. The Model With Vaccination

3.1. Presentation of the model with the control. In this section, we introduce a control variable $u_i^{C_j}$ that characterizes the effectiveness of the vaccination in the above mentioned model (1-3). This control in some situations can represent the effect of the awareness and media programs [18, 19].

In almost all infectious diseases, the authorities determine the threshold of risk based on many factors, such as availability of medical equipment, budgets, and medical personnel ... Thus, they can wait some time to see the course of events before the intervention. If the number of casualties exceeds this limit, decision-makers have no choice but to start trying to control the situation. This motivate us to define a Boolean function $\varepsilon_i^{C_j} = f^{C_j}(I)$ ($\varepsilon_i^{C_j} = 1$ or $\varepsilon_i^{C_j} = 0$) associated to domain C_j, that will be called the importance function of C_j. Where $\varepsilon_i^{C_j}$ is either equaling to 1, in the case when the number of infected of the cell C_j at instant i is greater than or equal to the threshold $\mathscr{I}^{C_j}$ defined by the authorities and health decision-makers, or $\varepsilon_i^{C_j} = 0$ otherwise. Therefore, we define the importance function $\varepsilon_i^{C_j}$ by the Heaviside step function H as follows

$$\varepsilon_i^{C_j} = H\left(I_i^{C_j} - \mathscr{I}^{C_j}\right) = \begin{cases} 0 & I_i^{C_j} < \mathscr{I}^{C_j} \\ 1 & I_i^{C_j} \geq \mathscr{I}^{C_j} \end{cases}$$

Then for a given domain $C_j \in \Omega$, the model is given by the following equations

$$\begin{aligned} S_{i+1}^{C_j} &= S_i^{C_j} - \sum_{C_k \in V(C_j)} \beta^{C_k}_{C_j} \frac{I_i^{C_k}}{N_i^{C_j}} S_i^{C_j} + \left(N_i^{C_j} - S_i^{C_j}\right) d_j \\ &\quad - \varepsilon_i^{C_j} u_i^{C_j} S_i^{C_j} \end{aligned} \tag{4}$$

$$I_{i+1}^{C_j} = I_i^{C_j} + \sum_{C_k \in V(C_j)} \beta^{C_k}_{C_j} \frac{I_i^{C_k}}{N_i^{C_j}} S_i^{C_j} - \gamma_j I_i^{C_j} - j I_i^{C_j} - \alpha^{C_j} I_i^{C_j} \tag{5}$$

$$R_{i+1}^{C_j} = R_i^{C_j} + \gamma_j I_i^{C_j} - d_j R_i^{C_j} + \varepsilon_i^{C_j} u_i^{C_j} S_i^{C_j} \tag{6}$$

Our goal is obviously to try to minimize the population of the susceptible group and the cost of vaccination in all affected regions. Our control functions taking values between $u_{min}^{C_j}$ and $u_{max}^{C_j}$, where $u_{min}^{C_j}, u_{max}^{C_j} \in]0,1[\,, \forall C_j \in \Omega$.

3.2. An optimal control approach. We devise in this paper an optimal control approach for each region with different importance functions $\varepsilon_i^{C_j}$, $j = 1, ..., M$. We characterize an optimal control that minimize the number of the infected people and maximize the ones in the removed category for all affected regions. Then, we are interested by minimizing the functional

$$J(u) = \sum_{k=1}^{M} \varepsilon_i^{C_k} J^{C_k}(u^{C_k}) \tag{7}$$

where $J^{C_k}(u^{C_k})$ is given by

$$\begin{aligned} J^{C_j}(u^{C_j}) &= \left(\alpha_I^{C_j} I_N^{C_j} - \alpha_R^{C_j} R_N^{C_j}\right) \\ &+ \sum_{i=0}^{N-1} \left(\alpha_I^{C_j} I_i^{C_j} - \alpha_R^{C_j} R_i^{C_j} + \frac{A^{C_j}}{2}(u_i^{C_j})^2\right) \end{aligned} \tag{8}$$

where $A^{C_j} > 0$, $\alpha_I^{C_j} > 0$, $\alpha_R^{C_j} > 0$ are the weight constants of control, the infected and the removed in region C_j respectively, and $u = \left(u^{C_1}, ..., u^{C_M}\right)$ where $u^{C_j} = \left(u_0^{C_j}, ..., u_{N-1}^{C_j}\right)$.
Here, our goal is to minimize the number of infected people, minimize the systemic costs attempting to increase the number of removed people in each C_j (with $\varepsilon_i^{C_j} = 1$). In other words, we are seeking an optimal control u^* such that

$$J(u^*) = min\{J(u)/u \in U\}$$

where U is the control set defined by

$$U = \{u = \left(u^{C_1}, ..., u^{C_M}\right)/u^{C_j} \in U^{C_j}, \forall C_j \in \Omega\}$$

with

$$U^{C_j} = \{u^{C_j} \text{ measurable}/u_{min}^{C_j} \leq u_i^{C_j} \leq u_{max}^{C_j}, i = 0, ..., N-1\}$$

where $u_{min}^{C_j} \in]0,1[$ and $u_{max}^{C_j} \in]0,1[$, $\forall C_j \in \Omega$. The sufficient condition for existence of an optimal control for the problem follows from theorem 1. At the same time, by using Pontryagin's Maximum Principle [40] we derive necessary conditions for our optimal control in theorem 2. For this purpose, we define the Hamiltonian as

$$
\begin{aligned}
\mathscr{H} &= \sum_{j=1}^{M} \varepsilon_i^{C_j}\left(\alpha_I^{C_j} I_i^{C_j} - \alpha_R^{C_j} R_i^{C_j} + \frac{A^{C_j}}{2}(u_i^{C_j})^2\right) \\
&+ \sum_{j=1}^{M} \varepsilon_i^{C_j}\left[\zeta_{1,i+1}^{C_j}\left[S_i^{C_j} - \sum_{C_k \in V(C_j)} \beta^{C_k}_{C_j} \frac{I_i^{C_k}}{N_i^{C_j}} S_i^{C_j}\right.\right. \\
&\quad \left. + \left(N_i^{C_j} - S_i^{C_j}\right) d_j - \varepsilon_i^{C_j} u_i^{C_j} S_i^{C_j}\right] \\
&+ \zeta_{2,i+1}^{C_j}\left[I_i^{C_j} + \sum_{C_k \in V(C_j)} \beta^{C_k}_{C_j} \frac{I_i^{C_k}}{N_i^{C_j}} S_i^{C_j}\right. \\
&\quad \left. - \gamma_j I_i^{C_j} - d_j I_i^{C_j} - \alpha^{C_j} I_i^{C_j}\right] \\
&+ \zeta_{3,i+1}^{C_j}\left[R_i^{C_j} + \gamma_j I_i^{C_j} - d_j R_i^{C_j} + \varepsilon_i^{C_j} u_i^{C_j} S_i^{C_j}\right]\Big] \qquad (9)
\end{aligned}
$$

Theorem 1. *(Sufficient conditions) For the optimal control problem given by (7) along with the state equations (4-6), there exists a control $u^* \in U$ such that*

$$J(u^*) = min\{J(u)/u \in U\}$$

Proof. See Dabbs, K [[41], Theorem 1]. □

Theorem 2. *(Necessary Conditions)*

Given the optimal control u^* and solutions S^{C_j*}, I^{C_j*} and R^{C_j*}, there exists $\zeta_{k,i}^{C_j}$, $i = 1...N$, $k = 1,2,3$, the adjoint variables satisfying the following equations

$$
\begin{aligned}
\Delta\zeta_{1,i}^{C_j} &= -\varepsilon_i^{C_j}\left[\left(1 - \sum_{C_k \in V(C_j)} \beta^{C_k}_{C_j} \frac{I_i^{C_k}}{N_i^{C_j}} - d_j - \varepsilon_i^{C_j} u_i^{C_j}\right)\zeta_{1,i+1}^{C_j}\right. \\
&\quad \left. + \sum_{C_k \in V(C_j)} \beta^{C_k}_{C_j} \frac{I_i^{C_k}}{N_i^{C_j}} \zeta_{2,i+1}^{C_j} + \varepsilon_i^{C_j} u_i^{C_j} \zeta_{3,i+1}^{C_j}\right] \qquad (10) \\
\Delta\zeta_{2,i}^{C_j} &= -\varepsilon_i^{C_j}\left[\alpha_I^{C_j} - \beta^{C_j}_{C_j} \frac{S_i^{C_j}}{N_i^{C_j}} \zeta_{1,i+1}^{C_j}\right. \\
&\quad \left. + \left(1 + \beta^{C_j}_{C_j} \frac{S_i^{C_j}}{N_i^{C_j}} - \gamma_j - d_j - \alpha^{C_j}\right)\zeta_{2,i+1}^{C_j} + \gamma_j \zeta_{3,i+1}^{C_j}\right] \qquad (11) \\
\Delta\zeta_{3,i}^{C_j} &= -\varepsilon_i^{C_j}\left[-\alpha_R^{C_j} + (1 - d_j)\,\zeta_{3,i+1}^{C_j}\right] \qquad (12)
\end{aligned}
$$

where $\zeta_{1,N}^{C_j}=0, \zeta_{2,N}^{C_j}=\varepsilon_i^{C_j}\alpha_I^{C_j}, \zeta_{3,N}^{C_j}=-\varepsilon_i^{C_j}\alpha_R^{C_j}$ *are the transversality conditions. In addition,*

$$u^*=\left(u^{C_1*},...,u^{C_M*}\right)$$

where $u^{C_j}=\left(u_0^{C_j},...,u_{N-1}^{C_j}\right)$*, is given by*

$$u_i^{C_j*}=min\left\{max\left\{u_{min}^{C_j},\frac{\left(\zeta_{1,i+1}^{C_j}-\zeta_{3,i+1}^{C_j}\right)S_i^{C_j}}{A^{C_{pq}}}\right\},u_{max}^{C_j}\right\},\ if\ \varepsilon_i^{C_j}=1 \tag{13}$$

$$u_i^{C_j*}=0,\ otherwise \tag{14}$$

Proof. Using Pontryagin's Maximum Principle [40], we obtain the following adjoint equations

$$\begin{aligned}
\Delta\zeta_{1,i}^{C_j} &= -\frac{\partial\mathscr{H}}{\partial S_i^{C_j}}= -\varepsilon_i^{C_j}\left[\left(1-\sum_{C_k\in V(C_j)}\beta^{C_k}_{C_j}\frac{I_i^{C_k}}{N_i^{C_j}}-d_j-\varepsilon_i^{C_j}u_i^{C_j}\right)\zeta_{1,i+1}^{C_j}\right.\\
&\quad\left.+\left(\sum_{C_k\in V(C_j)}\beta^{C_k}_{C_j}\frac{I_i^{C_k}}{N_i^{C_j}}\zeta_{2,i+1}^{C_j}+\varepsilon_i^{C_j}u_i^{C_j}\zeta_{3,i+1}^{C_j}\right)\right]\\
\Delta\zeta_{2,i}^{C_j} &= -\frac{\partial\mathscr{H}}{\partial I_i^{C_j}}= -\varepsilon_i^{C_j}\left[\alpha-\beta^{C_j}_{C_j}\frac{S_i^{C_j}}{N_i^{C_j}}\zeta_{1,i+1}^{C_j}\right.\\
&\quad\left.+\left(1+\beta^{C_j}_{C_j}\frac{S_i^{C_j}}{N_i^{C_j}}-\gamma_j-d_j-\alpha^{C_j}\right)\zeta_{2,i+1}^{C_j}+\gamma_{pq}\zeta_{3,i+1}^{C_j}\right]\\
\Delta\zeta_{3,i}^{C_j} &= -\frac{\partial\mathscr{H}}{\partial R_i^{C_j}}= -\varepsilon_i^{C_j}\left[-\alpha_R^{C_j}+(1-d_j)\,\zeta_{3,i+1}^{C_j}\right]
\end{aligned}$$

with $\zeta_{1,N}^{C_j}=0, \zeta_{2,N}^{C_j}=\varepsilon_i^{C_j}\alpha_I^{C_j}, \zeta_{3,N}^{C_j}=-\varepsilon_i^{C_j}\alpha_R^{C_j}$. To obtain the optimality conditions we take the variation with respect to control $u_i^{C_{pq}}$ and set it equal to zero and $\varepsilon_i^{C_j}=1$:

$$\frac{\partial\mathscr{H}}{\partial u_i^{C_j}}=A^{C_j}u_i^{C_j}-\zeta_{1,i+1}^{C_j}S_i^{C_j}+\zeta_{3,i+1}^{C_j}S_i^{C_j}=0$$

Then, we obtain the optimal control

$$u_i^{C_j}=\frac{\left(\zeta_{1,i+1}^{C_j}-\zeta_{3,i+1}^{C_j}\right)S_i^{C_j}}{A^{C_j}}$$

And

$$u_i^{C_j}=0,\text{ if }\varepsilon_i^{C_j}=0$$

Parameter	Description	Value
β	Infection rate	0.001
d	Birth and death rate	0.00001
γ	Recovery rate	0.00001
α	Death due to the infection	0.0001

TABLE 2. Parameters values of β, d, α and γ utilized for the resolution of all multi-regions discrete systems and then leading to simulations obtained from Fig.3 to Fig.26, with the initial populations given in Table 1.

By the bounds in U (and U^{C_j}) of the control, it is easy to obtain $u_i^{C_j*}$ in the following form

$$u_i^{C_j*} = min\left\{ max\left\{ u_{min}^{C_j}, \frac{\left(\zeta_{1,i+1}^{C_j} - \zeta_{3,i+1}^{C_j}\right) S_i^{C_j}}{A^{C_{pq}}} \right\}, u_{max}^{C_j} \right\}, \text{ if } \varepsilon_i^{C_j} = 1$$

$$u_i^{C_j*} = 0, \text{ otherwise}$$

□

4. NUMERICAL RESULTS

In this section, we present numerical simulations associated to the above mentioned optimal control problem. We write a code in $MATLAB^{TM}$ and simulated our results for several scenarios. The optimality systems is solved based on an iterative discrete scheme that converges following an appropriate test similar the one related to the Forward-Backward Sweep Method (FBSM). The state system with an initial guess is solved forward in time and then the adjoint system is solved backward in time because of the transversality conditions. Afterwards, we update the optimal control values using the values of state and co-state variables obtained at the previous steps. Finally, we execute the previous steps till a tolerance criterion is reached.

4.1. Area of interest. We chose the Casablanca-Settat region and the Rabat-Salé-Kénitra region as the studied area Ω in this paper because we are convinced that we can find some useful data to support our work. They are the most populated and dynamic regions of Morocco, which contain the Rabat city as the capital of Morocco and the seventh largest city in the country

with an urban population of around 580,000 inhabitants (2014) and a metropolitan population of more than 1.2 million inhabitants. It is also the capital of the administrative region of Rabat-Salé-Kénitra. They contain also the Casablanca city as the economic and industrial capital of Morocco because with its demographic growth and continuous development of the industrial sector, and the 14 other provinces (see Fig.1), in order to illustrate the objective of our work.

Fig.1 illustrates an example of discrete geographical zones of Casablanca-Settat and Rabat-Salé-Kénitra regions (Morocco) where $M = 16$, this image was originally made based on information from [42, 43, 44].

4.2. Geographical vicinity. A shape-file is a simple, non topological format for storing the geometric location and attribute information of geographic features. Geographic features in a shape-file can be represented by points, lines, or polygons (areas). The workspace containing shape-files may also contain database tables, which can store additional attributes that can be joined to a shape-file's features [45]. ArcMap is a central application used in ArcGIS software, where we can view and explore GIS database for our study area, and where we assign symbols and create map layouts for printing or publication. In this application we can represent geographic information as a set of layers and other elements in a map. Common map elements of a map include the data frame containing the map layers for a given extent [46]. Neighborhood tools create output values for each cell location based on the location value and the values identified in a specified neighborhood [47]. We use this tool to create the neighborhood $V(C_j)$ of each separated zone C_j within the area of interest Ω. For instance

$$V(C_{15}) = \{C_{12}, C_{13}, C_{16}\}$$

4.3. Initialization. Without loss of generality, we set the same infection threshold for all zones, therefore, hereafter we note $\mathscr{I}^{C_j}$ as I_{min}. We suppose as initial states in the area of interest Ω the following values:

Susceptible: The real populations given in Table 1.

Infected: 100 infections only in the city of Casablanca, and 0 for the others.

Recovered: We assume that $i = 0$ represents the first appearance of the epidemic, therefore,

FIGURE 2. Initial states. (a) Susceptible population. (b) Infected population. (c) Recovered population.

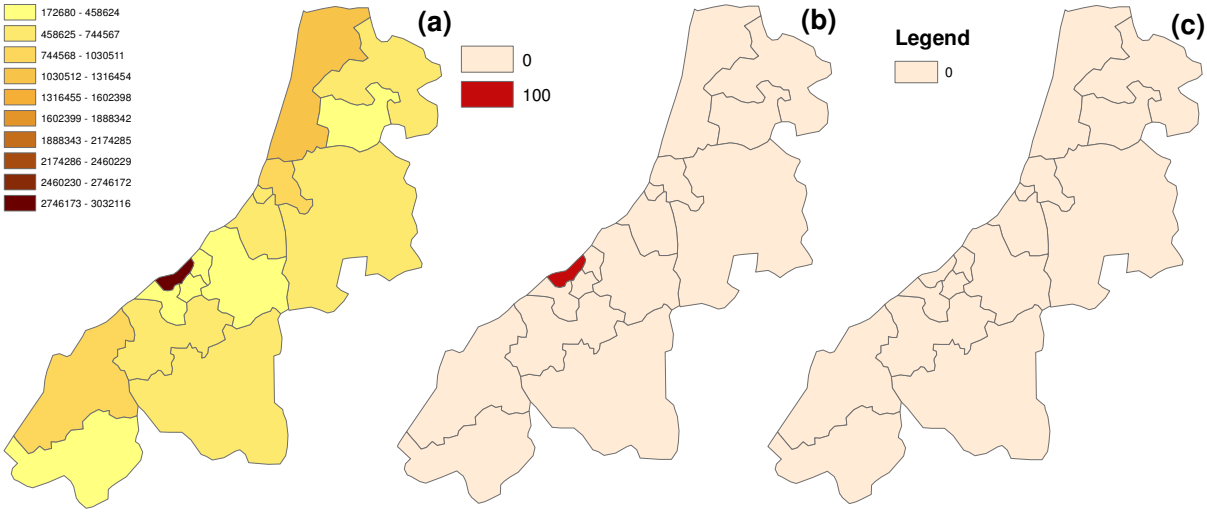

there are no recovered individuals.

Parameters: We use the parameters' values given in Table 2 for all zones.

Fig.2 represents the initial states of the multi-region SIR model of the 16 regions (zones) defined in the Fig.1. Fig.2 (a) defines in color the number of the initial states of susceptible in the 16 regions. The region of Casablanca named C_{15} is overcrowded with a population of about 3.5 million of citizens, then the region of Kenitra C_1 with a total population of approximately 1.5 million citizens, then the region of El Jadida C_9 with 1.2 million habitats, then the regions surrounding the metropolis C_{15} with populations which does not exceed 450,000 and the other regions of these two provinces which have an average population of around 700.000 citizens. Fig.2 (b) represents the initial state of the infected individuals in the different regions of the provinces of Casablanca-Settat and Rabat-Salé-Kénitra. It was assumed that only 100 cases of infected in the Casablanca C_{15} region and the other regions not infected yet. In Fig.2 (c) all regions have no recovered populations.

4.4. Scenario 0: Simulation of the multi-region model without any control. In all the rest geographical figures, we consider four time steps (a) $i = 50$, (b) $i = 100$, (c) $i = 150$, and (d) $i = 200$. Dark color represents the highest values. Geographical figures show the transmission of infection between different zones while associated graphs show states' changes over time.

FIGURE 3. Susceptible individuals without the control strategy.

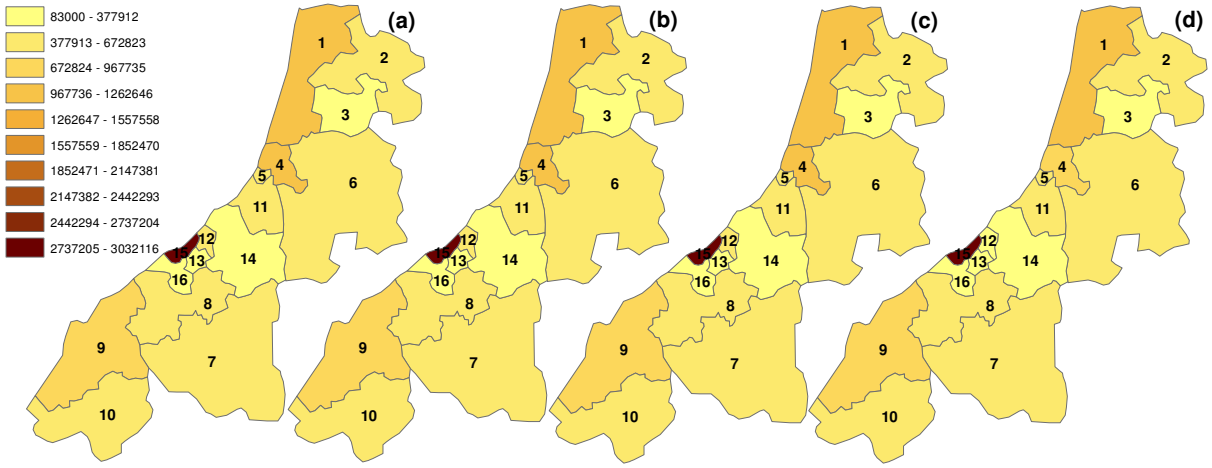

FIGURE 4. Temporal evolution of susceptible populations without the control strategy.

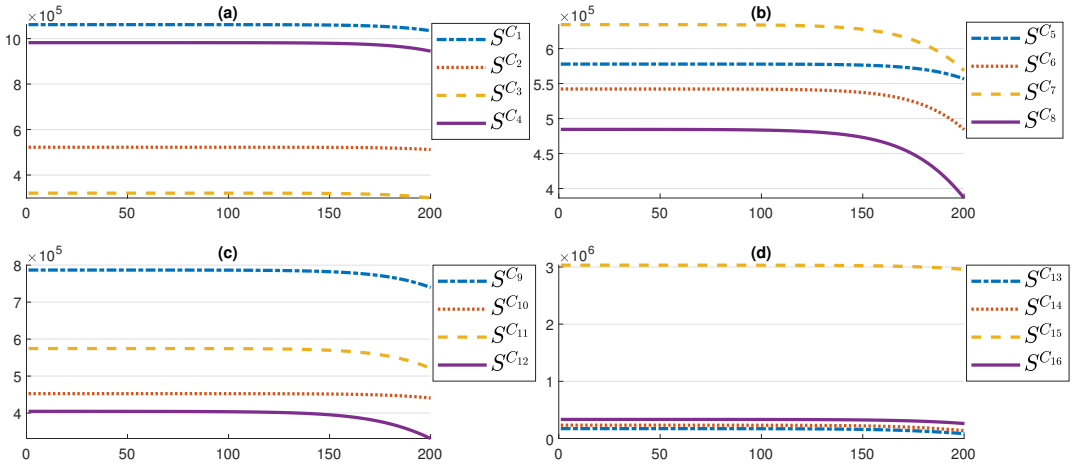

Fig.3.(a), (b), (c) and (d) indicate the geographical distribution of susceptible people in the 16 regions without any control strategy at the moments $i = 50$, $i = 100$, $i = 150$ and $i = 200$ respectively. While we see from Fig.4 that the number of susceptible people from regions C_6, C_7 and C_8 are constant until the instant $i = 150$ then decreases by about 1.10^5 person. In regions C_2, C_3 and C_{10} the number of susceptible people is almost constant throughout the period. The other regions experienced a slight decrease from time $i = 150$, due to the distance from the epidemic source.

Fig.5 and Fig.6 represent the evolution of the infected without controls in the different regions. We note that at the beginning, all the regions did not record any infection and that from the moment $i = 100$, the number of infected increases exponentially, especially for the regions

FIGURE 5. infected individuals without the control strategy

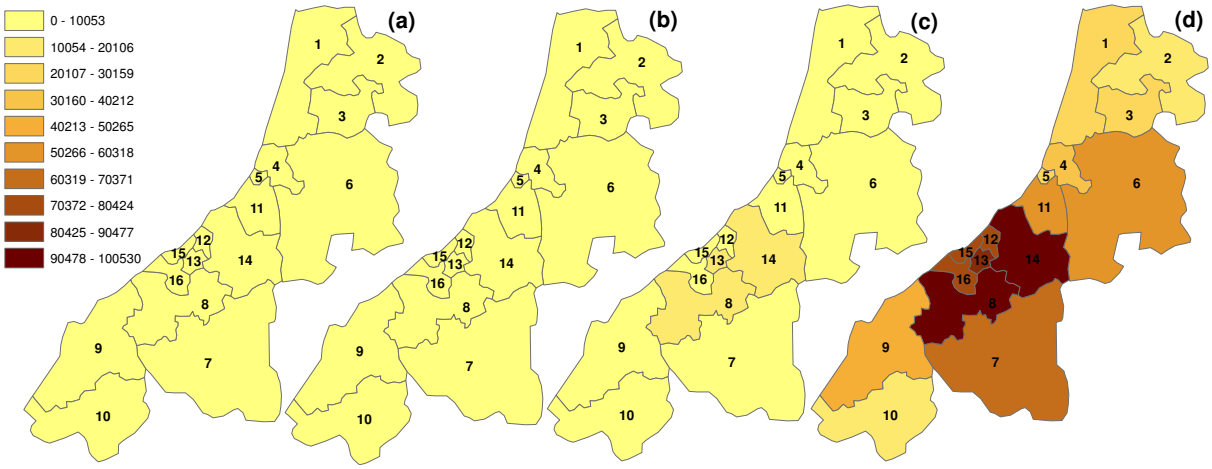

FIGURE 6. Temporal evolution of infected populations without the control strategy.

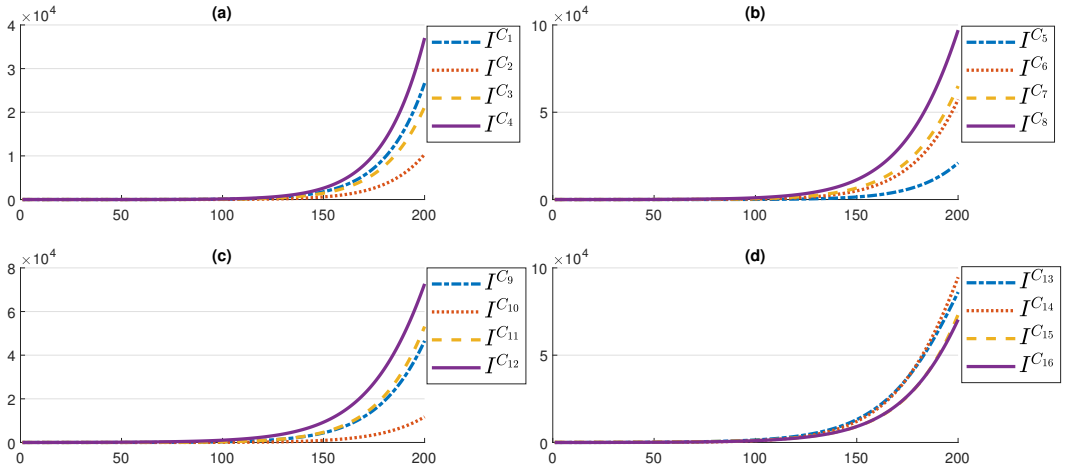

C_8, C_{13}, C_{14}, which surround the metropolis C_{15}, and which have reached a maximum value of 10^5 infected. The regions C_6, C_7, C_{12}, C_{15}, and C_{16} recorded about the instant $i = 200$ a maximum value which approaches the value 7.10^4, on the other hand, the regions C_9 and C_{11} reached 5.10^4 infected and the other regions haven't exceeded the number of 3.10^4 cases.

Figures 7 and 8 show the development of the recovered population without controls in the provinces of Casablanca-Settat and Rabat-Salé-Kénitra. We note that the numbers of the recovered, like the case of the infected, only change from the instant i = 100 and gradually increase to reach for the regions C_8, C_{13} and C_{14}, which surrounds the city of Casablanca, small values about the 220 recovered cases, while the C_6 and C_7 regions have reached about 130 recovered cases. C_9 and C_{11} reached at the end of the period about 100 recovered cases, and in the other

FIGURE 7. Recovered individuals without the control strategy

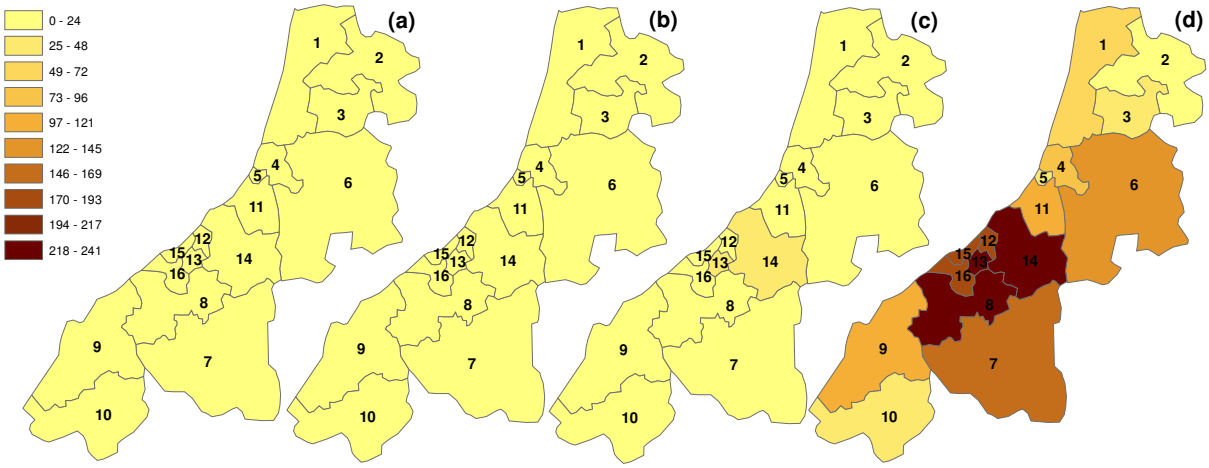

FIGURE 8. Temporal evolution of recovered populations without the control strategy.

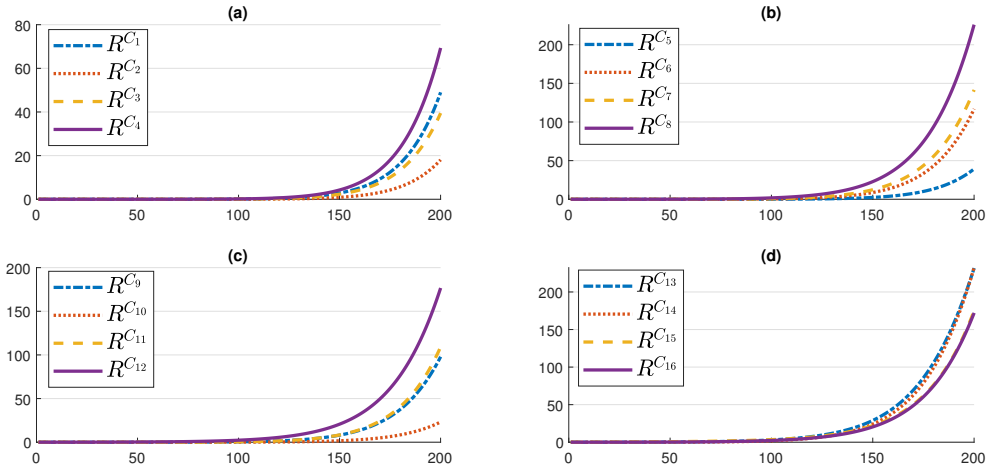

regions which are geographically further from C_{15} have do not exceed the 70 cases at the time $i = 200$.

These simulation show the necessity of some intervention to avoid these huge numbers of infections, especially in the epicenter of the epidemic and the surrounding zones.

4.5. Scenario 1: Application of the Vaccination control after detecting 1000 infections ($I_{min} = 1000$). Figures 9 and 10 show the evolution of the numbers of susceptible individuals in the 16 regions by applying the vaccination strategy in a zone after detecting 1000 infected in this zone . The regions C_8, C_{12}, C_{13}, C_{14}, C_{15}, and C_{16} surrounding the Casablanca region decrease rapidly from the moment $i = 100$. The regions which are less distant from C_{15} remain

FIGURE 9. Susceptible individuals with the vaccination control strategy where $I_{min} = 1000$.

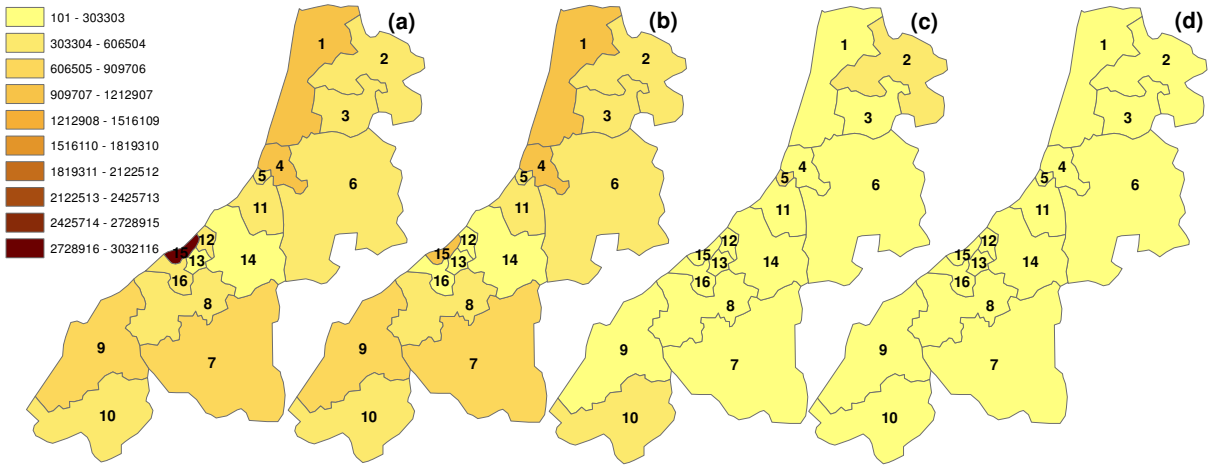

FIGURE 10. Temporal evolution of susceptible populations with the vaccination control strategy where $I_{min} = 1000$.

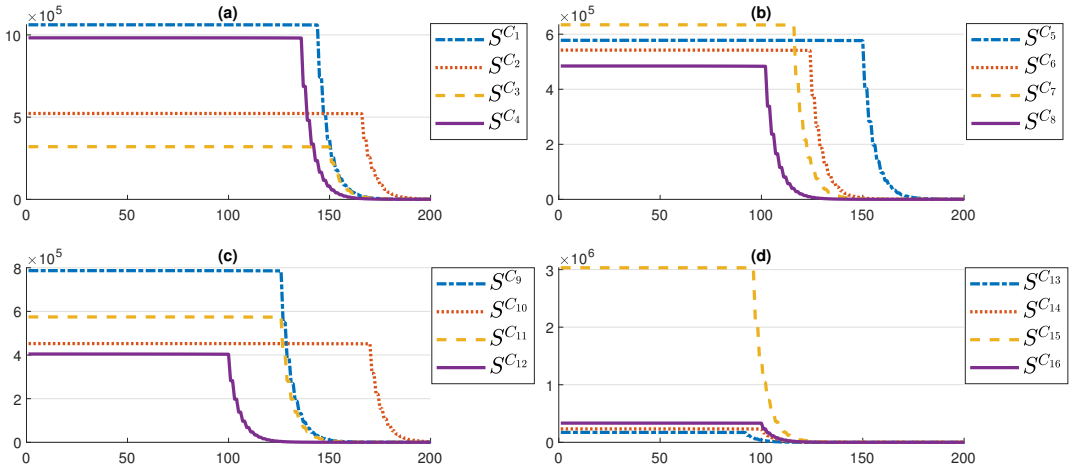

constant, then decrease rapidly towards 0. For regions C_1, C_3, C_4, and C_5, the susceptibles decrease very rapidly towards 0 from the moment $i = 150$. And finally, the regions C_2, and C_{10} which remain constant until $i = 175$, then converge towards 0. The number of susceptible with the vaccination strategy decreases very quickly towards zero once the number of infected exceeds 1000 cases in all regions, however without control it decreases by at most 10^5 cases or remains almost constant in some regions.

Fig.11 and Fig.12 represent the evolution of the numbers of infected cases in the 16 regions when applying the vaccination strategy from 1000 infected. The infections in regions C_8, C_{12},

FIGURE 11. Infected individuals with the vaccination control strategy where $I_{min} = 1000$.

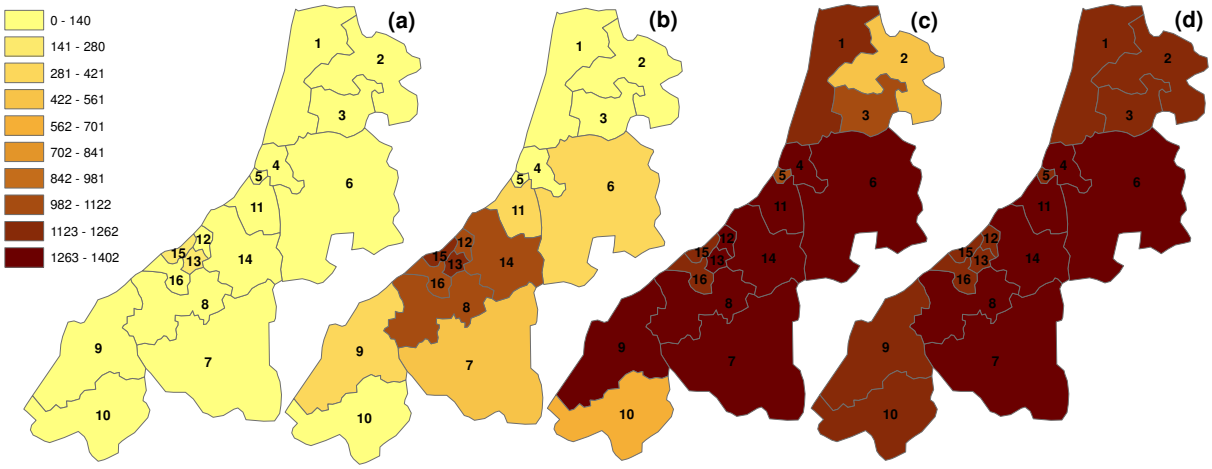

FIGURE 12. Temporal evolution of infected populations with the vaccination control strategy where $I_{min} = 1000$.

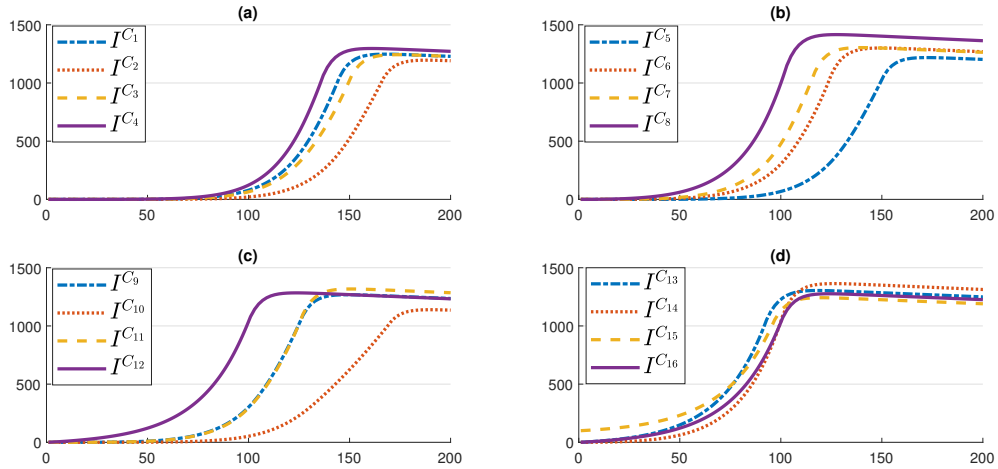

C_{13}, C_{14}, C_{15} and C_{16} begin to grow slowly from time $i = 50$ and then grow rapidly to reach its maximum value of almost 1350 cases infected at time $i = 100$. For regions C_6, C_7, C_9, C_{10} and C_{11}, reach their maximum value of 1200 cases at time i = 120 then decreases slightly and remains almost constant. The infected from regions C_1, C_3, C_4 and C_5 reach their maximum value of 1250 at time $i = 150$ and finally for regions C_{10} and C_2, the infected reach their maximum value at time $i = 175$ then remains constant until at the end of the vaccination campaign. once the number of infected exceeds 1000 cases in a region after reaching a certain time, the number of infected remains constant to be between 1200 and 1400 cases, on the other hand without

FIGURE 13. recovered individuals with vaccination control strategy where $I_{min} = 1000$.

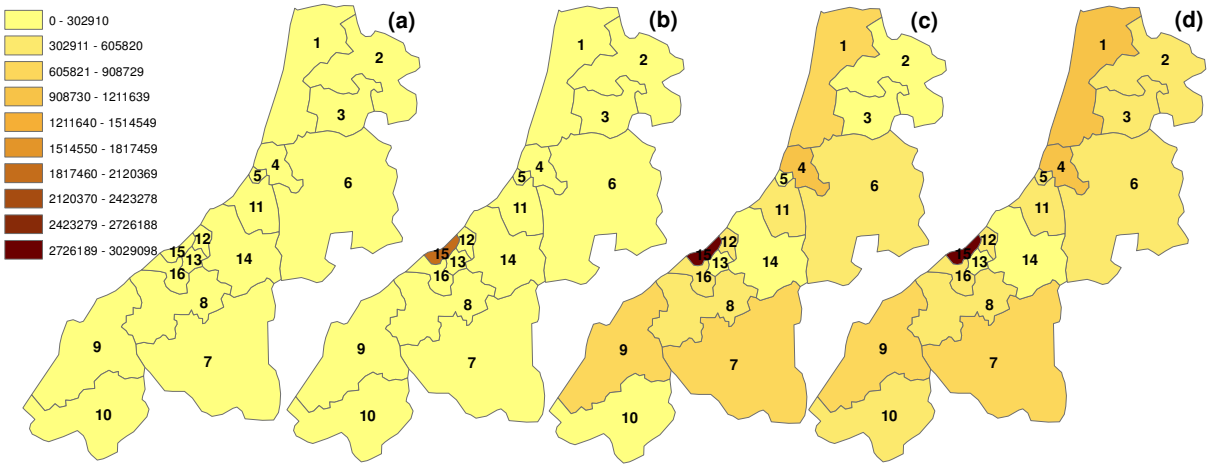

FIGURE 14. Temporal evolution of recovered populations with the vaccination control strategy where $I_{min} = 1000$.

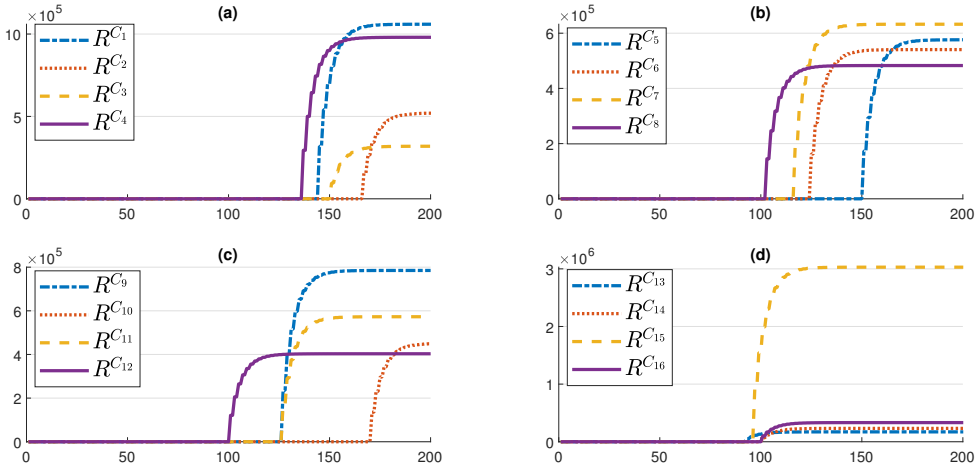

control it reaches very important values which exceeds 5.10^5 for regions bordering on region C_{15}.

Fig.13 and Fig.14 show the geographical progression and graphs of the cases recovered in the 16 regions by applying the vaccination strategy from 1000 infected. We observe that the regions closest to C_{15} begin to grow from the moment $i = 100$ and reach their maximum values between 3.10^5 and $4.8.10^5$ while the region C_{15} reaches the maximum of the recovered value at 3.10^6, the regions less far from C_{15} only grow from the moment $i = 125$ with maximum values between 5.10^5 and $5.85.10^5$. On the other hand, the farthest begins to grow at the instant $i = 150$

FIGURE 15. Susceptible individuals with the vaccination control strategy where $I_{min} = 500$

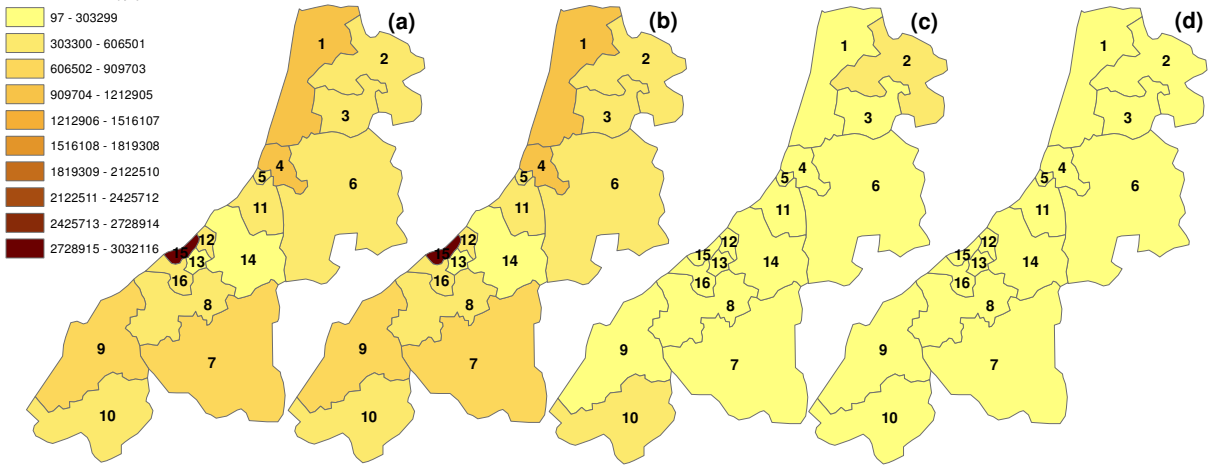

FIGURE 16. Temporal evolution of susceptible populations with the vaccination control strategy where $I_{min} = 500$.

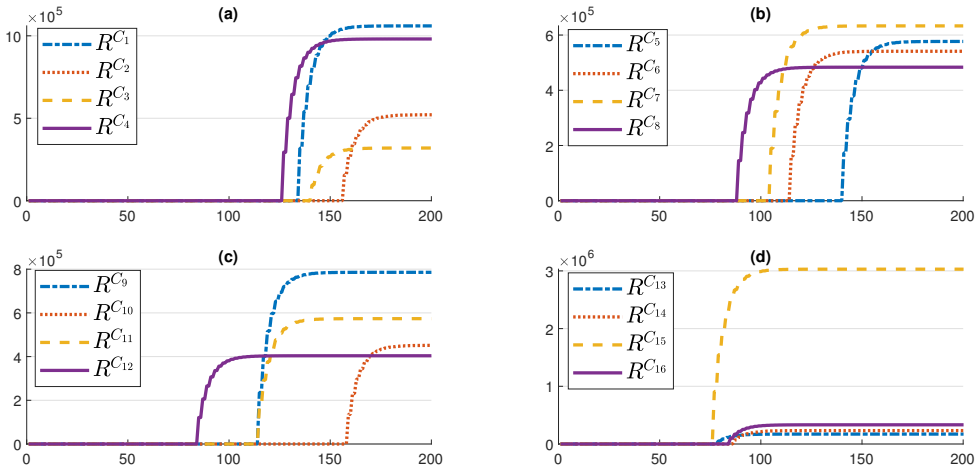

and the end regions increase from the instant $i = 170$ with recovered values between $4.3.10^5$ and 5.10^5. once the number of infected exceeds 1000 cases in a region after reaching a certain time, the number of recovered increases very quickly to reach a maximum value and remains constant after this value which exceeds 4.10^5 cases, however without control it does not exceed 200 boxes.

FIGURE 17. infected individuals with vaccination control strategy where $I_{min} = 500$.

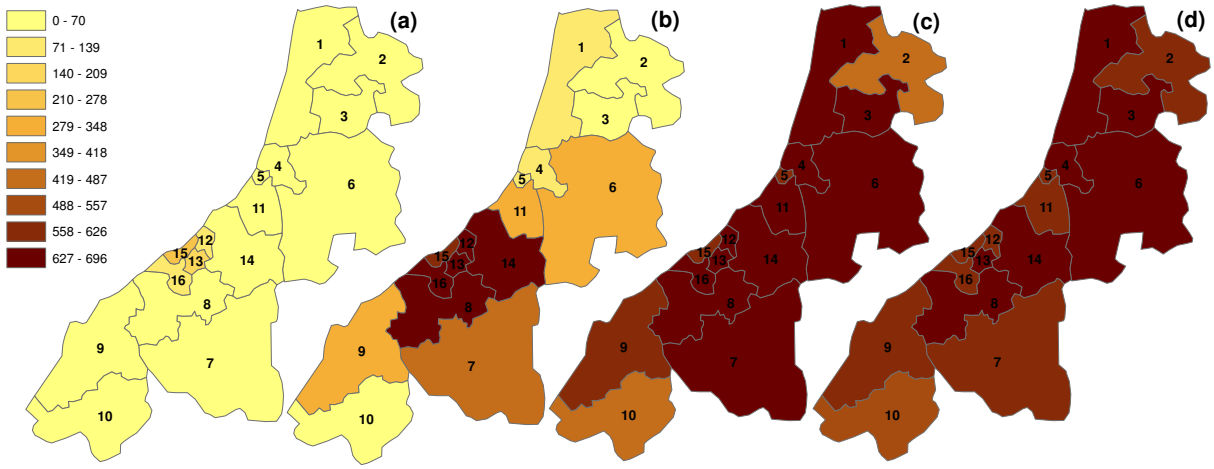

4.6. Scenario 2: Application of the Vaccination control after detecting 500 infections ($I_{min} = 500$). Fig.15 and Fig.16 show the evolution of susceptible people in the different regions by applying the vaccination strategy from 500 detected infection. The susceptible of the regions C_8, C_{12}, C_{13}, C_{14}, C_{15} and C_{16}, remain stable until the beginning the instant $i = 85$ then decreases rapidly towards 0. And each time we move away from the region C_{15}, the time that the numbers of the susceptible can take to converge towards 0 increases. So the susceptible of the region C_7 decreases towards 0 from $i = 100$, and the number of susceptible of the regions C_6, C_9, C_{11} tends to 0 from the time $i = 120$. Thus up to the regions C_2, C_5 and C_{10} whose number of susceptible decreases towards 0 at the moment $i = 150$. We also note that the number of susceptible individuals decreases over time less with the $I_{min} = 500$ strategy than with $I_{minj} = 1000$.

Fig.17 and Fig.18 show the geographical evolution and graphs of infections in the different regions by applying the vaccination strategy from 500 infected. All regions recognize the same evolution of its infections with the difference in time which begin to grow and the time which registers its maximum value which is counted between 600 and 650 infected. The closest areas to the city of Casablanca C_8, C_{12}, C_{13}, C_{14}, C_{15} and C_{16}, begin first from $i = 50$ and arrives at the peak at time $i = 100$. Then the regions C_3, C_4, C_6, C_7, C_9, C_{11}, the least close, its infections rise from the moment $i = 75$ and reach its maximum value at the instant $i = 120$, then, remain almost constant until the end of vaccination. After the infected regions C_2, C_5 and C_{10} begins to rise from time $i = 100$ and reaches its maximum value at the moment $i = 150$ with 600 infected.

FIGURE 18. Temporal evolution of infected populations with the vaccination control strategy where $I_{min} = 500$.

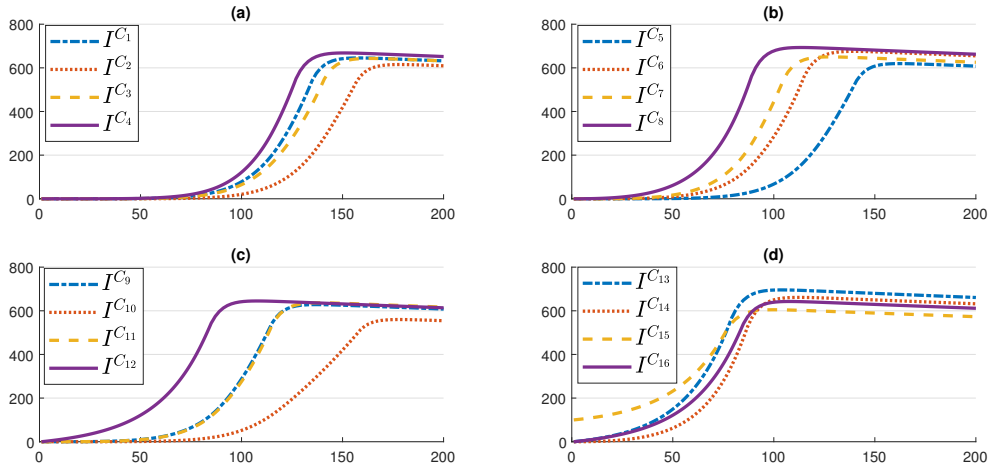

FIGURE 19. recovered individuals with vaccination control strategy where $I_{min} = 500$.

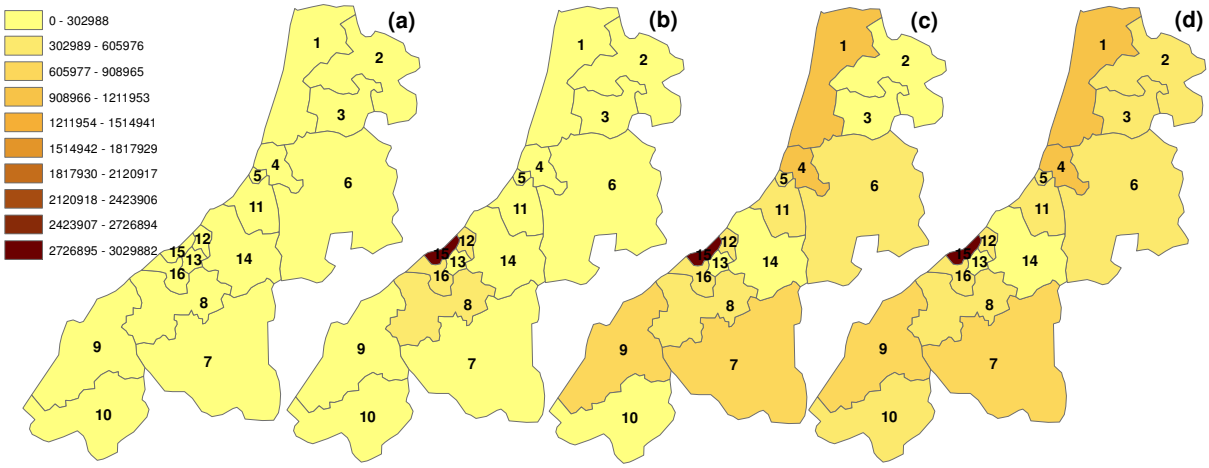

We also note that the number of infected is around 600 cases while with the vaccination strategy from 1000 infected the number exceeds 1200 cases.

Fig.19 and Fig.20 show the evolution of the recovered in the different regions by applying the vaccination strategy from 500 infected. We find that the number of recovered starts with zero at the beginning then begins to grow but from different periods and exceeds the number 3.10^5 of the recovered, which is more important than the recovered when there are no control strategies, which are at best reached the value than 200 cases. The regions closest to Casablanca start to grow from $i = 80$ and very quickly reach extreme values which exceed 3.10^5, then the

FIGURE 20. Temporal evolution of recovered populations with the vaccination control strategy where $I_{min} = 500$.

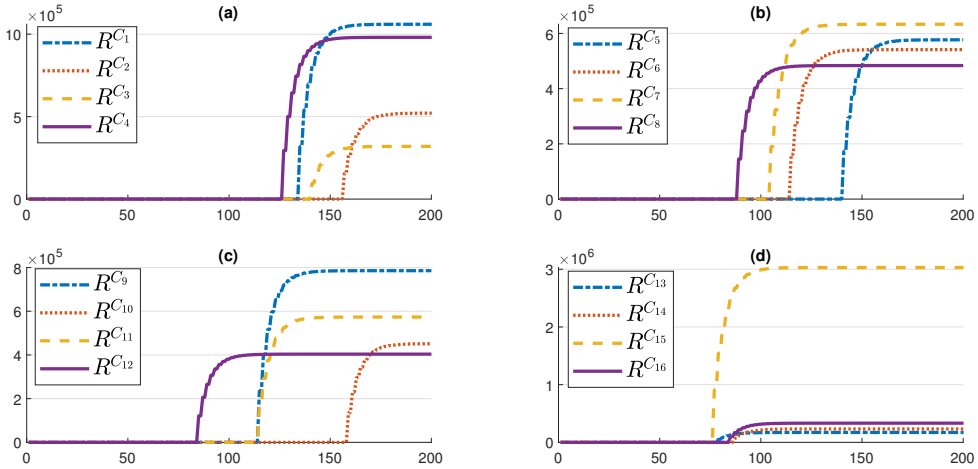

less distant regions which also grow rapidly from the time i = 130 and reach the maximum value on average of 8.10^5 and the most distant regions which grow from the instant $i = 160$ and reaches the value of $4.5.10^5$. We also note that the number of recovered is the same for the two vaccination strategies after 500 and 1000 with the difference that with 500 the number of recovered increases with a shorter time than with the vaccination strategy from 1000 infected.

4.7. Scenario 3: Application of the Vaccination control from the beginning of the epidemic ($I_{min} = 0$). In this scenario we assume that the epidemic is well known in other places, thus, we apply the control interventions from the declaration of such epidemic.

Fig.21 and Fig.22 represent the evolution of susceptible individuals in the 16 regions when applying the vaccination strategy without setting a threshold for infected cases. We note that all the regions except the metropolitan region C_{15} know an extreme fall of the susceptible populations, which is canceled very quickly from the instant $i = 25$. For the region C_{15} remains at the beginning constant with a value of 3.10^6, then decreases from the instant $i = 25$ and is canceled by the instant $i = 48$. Without the threshold for infected people, the susceptible decreases very quickly towards zero, however for the other strategies, the infected must reach the threshold set to begin to decrease.

Fig.23 and Fig.24 show the evolution of the infected in the 16 regions by applying the vaccination strategy from the beginning of the epidemic. The number of infections in all regions

FIGURE 21. Susceptible individuals with the vaccination control strategy where $I_{min} = 0$.

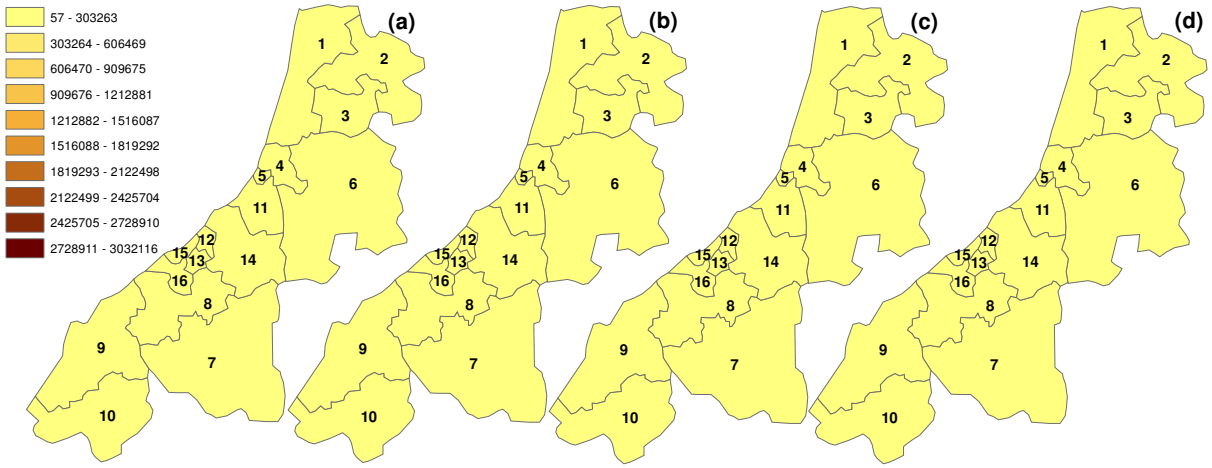

FIGURE 22. Temporal evolution of susceptible populations with the vaccination control strategy where $I_{min} = 0$.

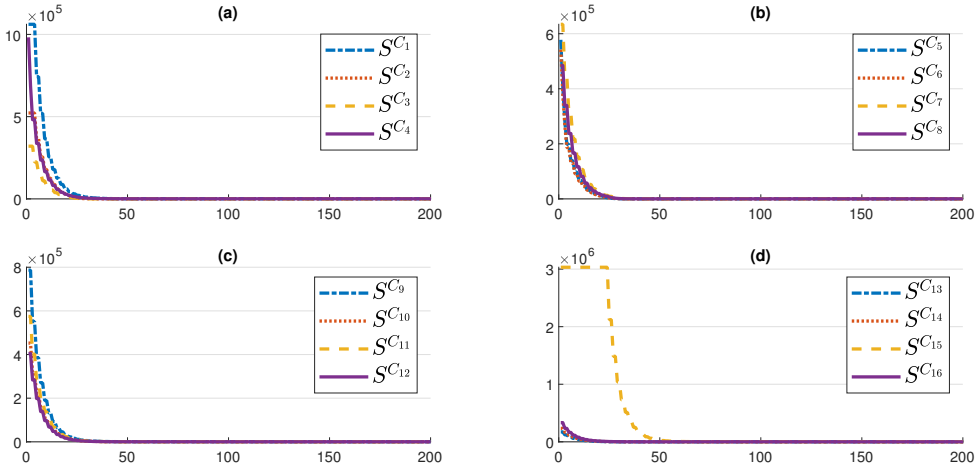

except regions C_{12}, C_{15} and C_{16} remains almost zero throughout the vaccination period. In the region C_{12} the number of infected increases from 0 to 7 infected from the moment $i = 25$ and remains in this value until the end of the vaccination. For region C_{15}, the number of infected rises from 100 cases to 135 at time $i = 25$ and then decreases slightly to reach the value of 120 cases at the end. The infected in the region have a weak growth of 10 cases from times $i = 10$ and remains constant until the end. Without the threshold of infected, the number of infected does not exceed 130 cases, but the cost will be very high than those of the other two scenarios.

FIGURE 23. Infected individuals with vaccination control strategy where $I_{min} = 0$.

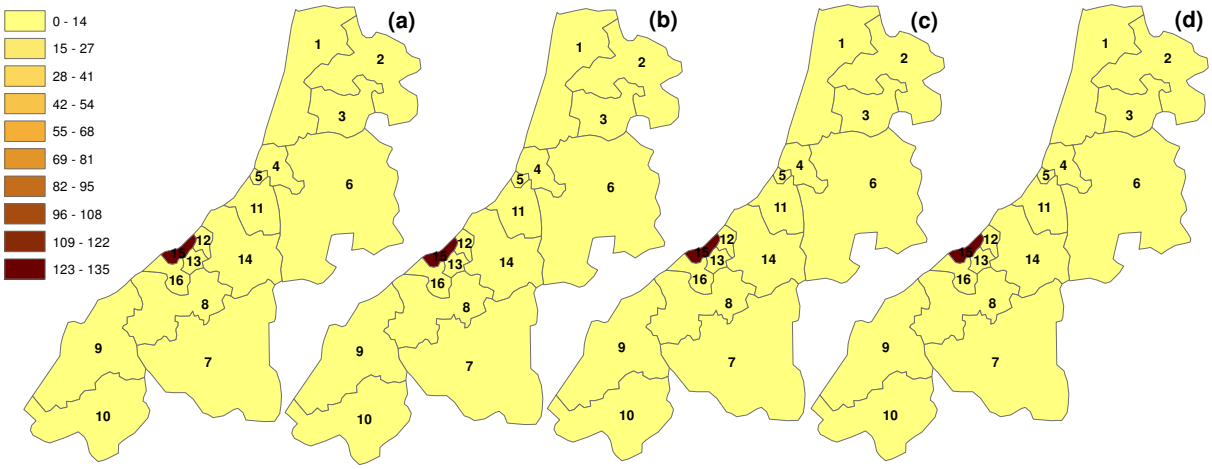

FIGURE 24. Temporal evolution of infected populations with the vaccination control strategy where $I_{min} = 0$.

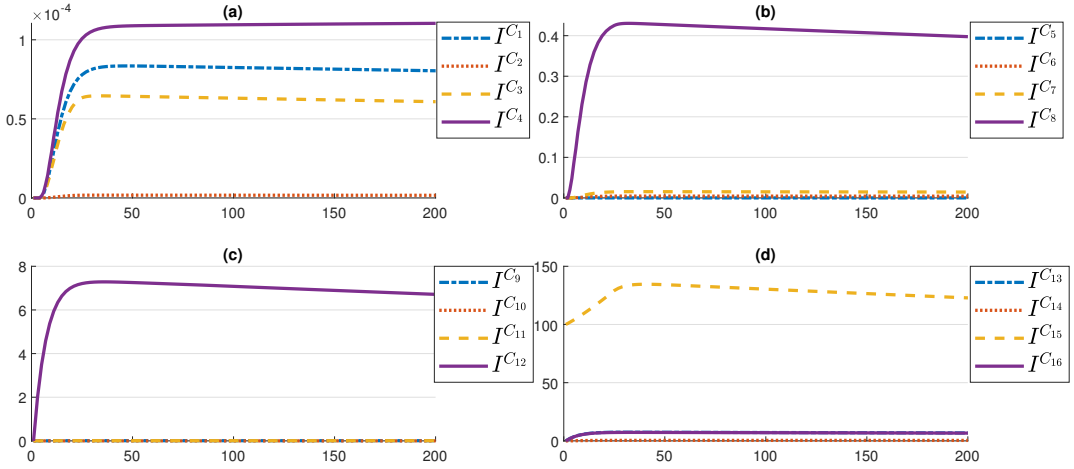

Fig.25 and Fig.26 show the geographical evolution and graphs of the recovered populations in the 16 regions by applying the vaccination strategy without setting any threshold of infection. All regions except the region C_{15} recognize a progression of these recoveries from the start to reach maximum values at the instant $i = 25$ and remain constant throughout the period of control. On the other hand, for C_{15} it remains almost zero at the beginning until the time $i = 25$ to starts to grow and reaches its maximum value about 3.10^6 at the instant $i = 50$, and then remains constant until the end of the period of vaccination. Without the infected threshold, the recovered quickly grows towards its maximum value, however for the other two scenarios take some time to increase.

FIGURE 25. recovered individuals with vaccination control strategy where $I_{min} = 0$.

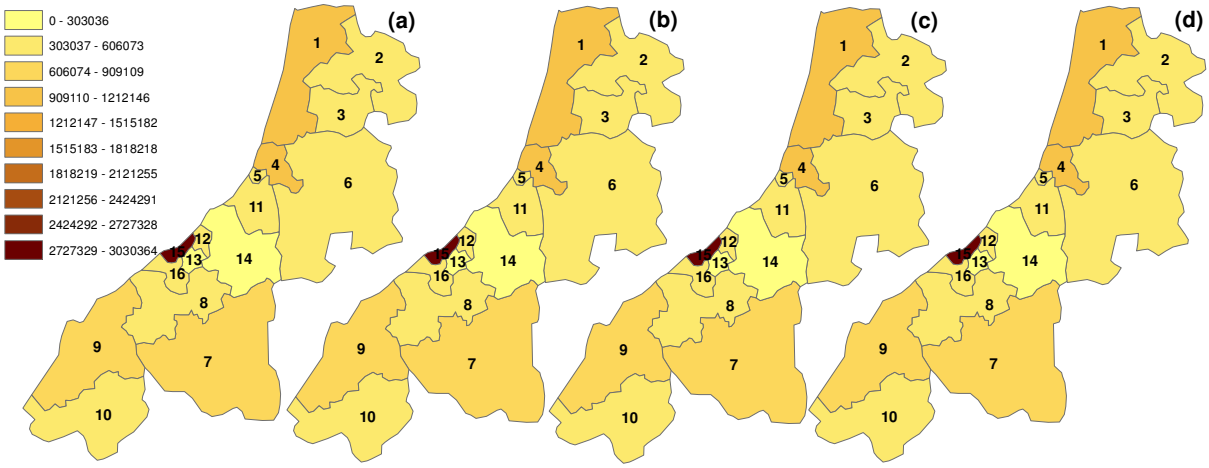

FIGURE 26. Temporal evolution of recovered populations with the vaccination control strategy where $I_{min} = 0$.

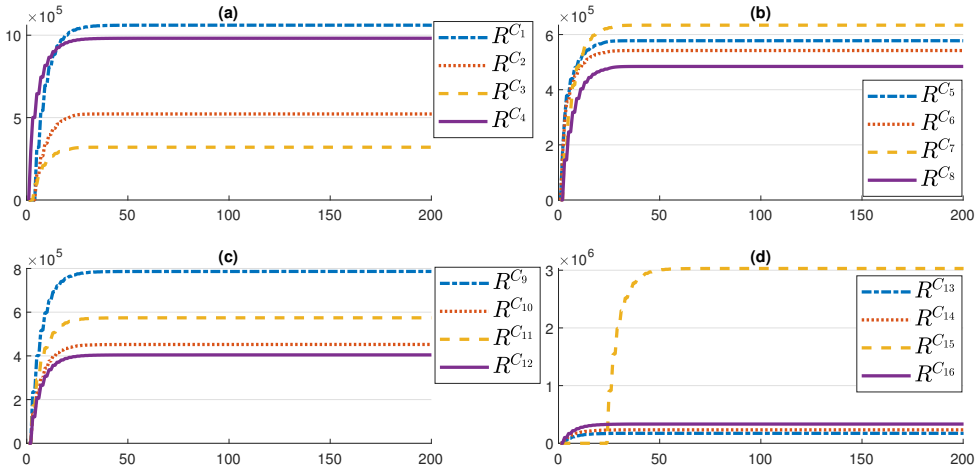

5. CONCLUSION

In this paper, we devised a novel optimization approach that represents an extension of the optimal control approach studied in the work of Zakary et al. in the paper [35]. We applied this new approach to a multi-region discrete epidemic model which has been firstly proposed in [7]. We suggested in this article, a new analysis of infection dynamics in M regions which we supposed to be accessible for health authorities. By defining new importance functions to identify affected zones and then will be treated. We investigated the effectiveness of optimal vaccination

control approach, we introduced into the model, control functions associated with appropriate control strategies followed in the targeted regions by mass vaccination campaigns by considering different scenarios. Based on our numerical simulations, we showed the geographical spread of the epidemic and the influence of each region on another and then we deduced the effectiveness of each strategy followed. We concluded that the last scenario of optimal control approach when $I_{min} = 0$ has given better results than the other cases regarding the maximization of the number of removed individuals and minimization of the spread of infection in all regions studied, but this is clearly the most expensive scenario. Thus, as a result, it is necessary to define small thresholds to control the situation as much as possible.

DATA AVAILABILITY

Data of the actual populations of the Casablanca-Settat region from [43] and for the Rabat-Salé-Kénitra region from [44].

CONFLICT OF INTERESTS

The author(s) declare that there is no conflict of interests.

FUNDING STATEMENT

The author(s) received no financial support for the research, authorship, and/or publication of this article

REFERENCES

[1] N. C. Grassly, C. Fraser, Mathematical models of infectious disease transmission, Nat. Rev. Microbiol. 6 (6) (2008), 477–487.

[2] K. Dietz, D. Schenzle, Mathematical models for infectious disease statistics, in: A celebration of statistics, Springer, 1985, pp. 167–204.

[3] J. C. Frauenthal, Mathematical modeling in epidemiology, Springer, 2012.

[4] H. Hethcote. A thousand and one epidemic models. In: Levin, S. (eds) Frontiers in Mathematical Biology, pp 504–515. Springer, Berlin, 1994.

[5] O. Diekmann, Heesterbeek, J.A.P.: Mathematical Epidemiology of Infectious Diseases: Model Building, Analysis and Interpretation. Wiley, Chichester, 2000.

[6] L. J. Allen, A primer on stochastic epidemic models: Formulation, numerical simulation, and analysis, Infect. Dis. Model. 2 (2) (2017), 128–142.

[7] O. Zakary, M. Rachik, I. Elmouki, On the analysis of a multi-regions discrete sir epidemic model: an optimal control approach, Int. J. Dyn. Control. 5 (3) (2017), 917–930.

[8] A. A. Toda, Susceptible-Infected-Recovered (SIR) Dynamics of COVID-19 and Economic Impact, ArXiv:2003.11221 [Econ, q-Bio, q-Fin]. (2020).

[9] P. Shu, W. Wang, M. Tang, Y. Do, Numerical identification of epidemic thresholds for susceptible-infected-recovered model on finite-size networks, Chaos. 25 (2015), 063104.

[10] E. Volz, L. A. Meyers, Susceptible–infected–recovered epidemics in dynamic contact networks, Proc. R. Soc. B. Biol. Sci. 274 (1628) (2007), 2925–2934.

[11] A. A. Nash, R. G. Dalziel, J. R. Fitzgerald, Mims' pathogenesis of infectious disease, Academic Press, New York, 2015.

[12] D. Greenwood, R. C. Slack, M. R. Barer, W. L. Irving, Medical Microbiology E-Book: A Guide to Microbial Infections: Pathogenesis, Immunity, Laboratory Diagnosis and Control. With STUDENT CONSULT Online Access, Elsevier Health Sciences, 2012.

[13] B. Sara, Z. Omar, T. Abdessamad, R. Mostafa, F. Hanane, Parameters' estimation, sensitivity analysis and model uncertainty for an influenza a mathematical model: case of morocco, Commun. Math. Biol. Neurosci. 2020 (2020), 57.

[14] Y. Zhou, Z. Ma, F. Brauer, A discrete epidemic model for sars transmission and control in china, Math. Computer Model. 40 (13) (2004), 1491–1506.

[15] M. I. Meltzer, I. Damon, J. W. LeDuc, J. D. Millar, Modeling potential responses to smallpox as a bioterrorist weapon, Emerg. Infect. Dis. 7 (6) (2001), 959–969.

[16] O. Zakary, S. Bidah, M. Rachik, The impact of staying at home on controlling the spread of covid-19: Strategy of control, Mexican J. Biomed. Eng. 42 (1) (2020), 10–26.

[17] O. Zakary, H. Ferjouchia, S. Bidah, M. Rachik, et al. Mathematical modeling of public opinions: Parameter estimation, sensitivity analysis, and model uncertainty using an agree-disagree opinion model, Abstr. Appl. Anal. 2020 (2020), 1837364.

[18] O. Zakary, M. Rachik, I. Elmouki, A multi-regional epidemic model for controlling the spread of ebola: awareness, treatment, and travel-blocking optimal control approaches, Math. Meth. Appl. Sci. 40 (4) (2017), 1265–1279.

[19] O. Zakary, A. Larrache, M. Rachik, I. Elmouki, Effect of awareness programs and travel-blocking operations in the control of hiv/aids outbreaks: a multi-domains sir model, Adv. Differ. Equ. 2016 (2016), 169.

[20] H. Boutayeb, S. Bidah, O. Zakary, M. Rachik, A new simple epidemic discrete-time model describing the dissemination of information with optimal control strategy, Discr. Dyn. Nat. Soc. 2020 (2020), 7465761.

[21] Z. Rachik, H. Boutayeb, S. Bidah, O. Zakary, M. Rachik, Control of information dissemination in online environments: optimal feedback control, Commun. Math. Biol. Neurosci. 2020 (2020), 86.

[22] Z. Rachik, S. Bidah, H. Boutayeb, O. Zakary, M. Rachik, Understanding the different objectives of information and their mutual impact: multi-information model, Commun. Math. Biol. Neurosci. 2021 (2021), 1.

[23] M. Roberts, M. Tobias, Predicting and preventing measles epidemics in new zealand: application of a mathematical model, Epidemiol. Infect. 124 (2) (2000), 279–287.

[24] R. M. Granich, C. F. Gilks, C. Dye, K. M. De Cock, B. G. Williams, Universal voluntary hiv testing with immediate antiretroviral therapy as a strategy for elimination of hiv transmission: a mathematical model, Lancet 373 (9657) (2009), 48–57.

[25] S. Gupta, J. Swinton, R. M. Anderson, Theoretical studies of the effects of heterogeneity in the parasite population on the transmission dynamics of malaria, Proc. R. Soc. Lond. Ser. B. Biol. Sci. 256 (1347) (1994), 231–238.

[26] M. Lhous, O. Zakary, M. Rachik, E. M. Magri, A. Tridane, Optimal containment control strategy of the second phase of the covid-19 lockdown in morocco, Appl. Sci. 10 (21) (2020), 7559.

[27] D. Kang, H. Choi, J.-H. Kim, J. Choi, Spatial epidemic dynamics of the covid-19 outbreak in China, Int. J. Infect. Dis. 94 (2020), 96-102.

[28] I. A. Adekunle, A. Onanuga, O. Wahab, O. O. Akinola, Modelling spatial variations of coronavirus disease (COVID-19) in Africa, Sci. Total Environ. 729 (2020), 138998

[29] O. Zakary, S. Bidah, M. Rachik, H. Ferjouchia, Mathematical model to estimate and predict the covid-19 infections in morocco: Optimal control strategy, J. Appl. Math. 2020 (2020), 9813926.

[30] J. N. Hays, Epidemics and Pandemics: Their Impacts on Human History. ABC-CLIO. Santa Barbara, CA, 2005.

[31] J. Reidl, K. E. Klose, Vibrio cholerae and cholera: out of the water and into the host, FEMS Microbiol. Rev. 26 (2) (2002), 125–139.

[32] C. D. Butler, Nature, gaia, plagues, and people: Three books on a path to ecohealth, EcoHealth, 9 (3) (2012), 363–364.

[33] N. S.-N. Lam, M. Fan, K.-b. Liu, Spatial-temporal spread of the aids epidemic, 1982–1990: A correlogram analysis of four regions of the united states, Geogr. Ana. 28 (2) (1996), 93–107.

[34] P. Lemey, M. Suchard, A. Rambaut, Reconstructing the initial global spread of a human influenza pandemicA Bayesian spatial-temporal model for the global spread of H1N1pdm, PLoS Curr. 1 (2009), RRN1031.

[35] O. Zakary, M. Rachik, I. Elmouki, A new analysis of infection dynamics: multi-regions discrete epidemic model with an extended optimal control approach, Int. J. Dyn. Control. 5 (4) (2017), 1010–1019.

[36] I. Abouelkheir, M. Rachik, O. Zakary, I. Elmouk, A multi-regions sis discrete influenza pandemic model with a travel-blocking vicinity optimal control approach on cells, Amer. J. Comput. Appl. Math. 7 (2) (2017), 37–45.

[37] L. Abu-Raddad, F. A. Akala, I. Semini, G. Riedner, D. Wilson, O. Tawil, Characterizing the HIV/AIDS epidemic in the Middle East and North Africa: time for strategic action, The World Bank, Washington, 2010.

[38] D. Bundy, A. Patrikios, C. Mannathoko, A. Tembon, S. Manda, B. Sarr, L. Drake, Accelerating the education sector response to HIV: Five years of experience from Sub-Saharan Africa, The World Bank, Washington, 2010.

[39] O. Zakary, M. Rachik, I. Elmouki, On the impact of awareness programs in hiv/aids prevention: an sir model with optimal control, Int. J. Comput. Appl. 133 (9) (2016), 1–6.

[40] L. S. Pontryagin, Mathematical theory of optimal processes, Routledge, 2018.

[41] K. Dabbs, Optimal control in discrete pest control models, Chancellor's Honors Program Projects. https://trace.tennessee.edu/utk_chanhonoproj/1375, (2010).

[42] Nouveau découpage territorial du royaume?, http://www.pncl.gov.ma/fr/News/Alaune/Pages/Nouveau-d%C3%A9coupage-r%C3%A9gional-du-Royaume-.aspx (2015).

[43] Recensement general de la population et de l'habitat 2014, https://www.hcp.ma/reg-casablanca/attachment/673830/ (2015).

[44] La région de rabat-salé-kénitra, http://www.pncl.gov.ma/fr/LesCollectivit%C3%A9sterritoriales/Documents/MONOGRAPHIE%20DE%20LA%20REGION%20DE%20RABAT%20SALE%20%20KENITRA%20FR.pdf (2015).

[45] What is a shapefile?, https://desktop.arcgis.com/en/arcmap/latest/manage-data/shapefiles/what-is-a-shapefile.htm (2020).

[46] what is arcmap?, https://desktop.arcgis.com/fr/arcmap/10.3/main/map/what-is-arcmap-.htm (2020).

[47] an overview of the neighborhood tools, https://desktop.arcgis.com/en/arcmap/10.3/tools/spatial-analyst-toolbox/an-overview-of-the-neighborhood-tools.htm (2020).